



OPEN ACCESS

EDITED BY
Jiang Bian,
Yangtze University, ChinaREVIEWED BY
Hongtao Li,
Southwest Petroleum University, China
Dan Jiang,
University of Electronic Science and
Technology of China, China*CORRESPONDENCE
Yudong Mao,
✉ maoyudong@sdjzu.edu.cnRECEIVED 24 November 2025
REVISED 31 January 2026
ACCEPTED 09 February 2026
PUBLISHED 13 March 2026

CITATION

Xu L, Cheng P, Li G, Wang N, Song J,
Xin G and Mao Y (2026) Research on
pneumatic hammer effect and transient
structural response characteristics of
natural gas pipeline in gas turbine based
on coupled fluid-structure interaction
simulations.
Front. Energy Res. 14:1751161.
doi: 10.3389/fenrg.2026.1751161

COPYRIGHT

© 2026 Xu, Cheng, Li, Wang, Song, Xin
and Mao. This is an open-access article
distributed under the terms of the
[Creative Commons Attribution License
\(CC BY\)](https://creativecommons.org/licenses/by/4.0/). The use, distribution or
reproduction in other forums is
permitted, provided the original
author(s) and the copyright owner(s) are
credited and that the original
publication in this journal is cited, in
accordance with accepted academic
practice. No use, distribution or
reproduction is permitted which does
not comply with these terms.

Research on pneumatic hammer effect and transient structural response characteristics of natural gas pipeline in gas turbine based on coupled fluid-structure interaction simulations

Lei Xu¹, Peng Cheng¹, Guanpeng Li¹, Nini Wang¹, Juxing Song¹,
Gongming Xin² and Yudong Mao^{3*}¹Shandong Electric Power Engineering Consulting Institute Corp., Ltd., Jinan, Shandong, China,
²School of Nuclear Science, Energy and Power Engineering, Shandong University, Jinan, Shandong,
China, ³School of Thermal Engineering, Shandong Jianzhu University, Jinan, China

As a core component of the fuel supply system, the natural gas pipeline of a gas turbine is responsible for the stable delivery of high-pressure gas during start-up and load regulation. With the increasing penetration of renewable energy into power grids, gas turbines are required to operate more frequently under start–stop conditions and rapid load fluctuations. As a result, valve operations in fuel supply pipelines occur more frequently, inducing transient pressure surges that may threaten system safety. The evolution of pneumatic hammer is strongly affected by gas compressibility, valve opening characteristics, and pipeline structural properties. Therefore, a clear understanding of pneumatic hammer propagation and the associated transient structural response under sudden flow variations is essential. In this study, a 300 MW-class F-type heavy-duty gas turbine fuel supply pipeline system is investigated. A fully coupled fluid–structure interaction model is established based on computational fluid dynamics and transient structural dynamics to analyze pressure wave propagation and pipeline structural responses under different valve opening strategies. The results show that, unlike liquid hammer, pneumatic hammer in natural gas pipelines does not exhibit an initial sharp pressure peak but instead features a long-period decay process. The pressure peak typically occurs as the valve approaches the fully open position, followed by multi-cycle oscillations caused by rarefaction waves and reflection interference. Both the valve opening duration and opening pattern significantly influence the pneumatic hammer intensity and structural response. Appropriately extending the valve opening time or optimizing the opening pattern can effectively reduce peak gas pressure and equivalent structural stress, thereby mitigating pipeline vibration. From a phase-response perspective, pipeline stress is nearly in phase with the pressure wave, whereas the pipe supports exhibit a time lag of approximately 0.2 s accompanied by dynamic amplification. High stress is localized at connection edges, while the overall structural stress remains below the allowable material limit, indicating good system safety. This study provides theoretical guidance

and engineering references for valve control optimization, pipeline support design, and the safe operation of gas turbine natural gas supply systems.

KEYWORDS

computational fluid dynamics, heavy-duty gas turbines, peak-adjustment of electric power system, pneumatic hammer effect, transient structural response

1 Introduction

As the core link of fuel supply in gas turbines, the natural gas pipeline system is responsible for stably delivering high-pressure natural gas to the combustion chamber during start-up, shutdown, and load adjustment processes. Through the coordinated operation of valves, pressure regulating devices, and distribution networks, this system evenly distributes high-pressure natural gas to each burner, thereby ensuring the efficient combustion and safe operation of the gas turbine. In recent years, with the rapid implementation and continuous increase in the power grid connection ratio of new energy power plants such as nuclear power, wind power, and photovoltaic power, the demand for peak shaving and frequency regulation in the power system has been increasing day by day (Islam et al., 2024; Verástegui et al., 2021; Fan et al., 2021; Impram et al., 2020). Gas turbines, with their advantages of flexible start-stop and rapid ramp-up, have gradually become an important force in supporting the consumption of new energy and the stable operation of power grids (Li et al., 2025; Yao et al., 2024; Ricci et al., 2021). However, this operating role also leads to frequent start-stop cycles and rapid load adjustments, resulting in more intensive and abrupt valve operations in natural gas pipeline systems. Such operating conditions are markedly different from those of conventional gas transmission pipelines and can induce strong transient gas pressure surges, whose associated pressure fluctuations and structural vibrations pose serious threats to pipeline integrity, combustion stability, and safe unit operation (Zha et al., 2024; Ding and Ji, 2023).

The pneumatic hammer effect is essentially a pressure wave propagation phenomenon resulting from the combined action of fluid inertia and compressibility (Di et al., 2025; Plouraboué, 2024). In natural gas pipelines, rapid valve opening or closure can cause abrupt changes in flow velocity, thereby triggering intense pressure fluctuations. This transient impact may not only lead to seal failure at pipeline joints, local plastic deformation, and damage to hanger supports (Zha et al., 2024; Riasi and Tazraei, 2017), but may also disturb gas flow distribution, inducing unstable combustion, flameout, or oscillation phenomena. Existing studies have demonstrated that factors such as fluid compressibility (Plouraboué, 2024; Ren et al., 2020) and valve operating characteristics (Xin et al., 2024; Yao et al., 2015; Mo et al., 2021; Davies et al., 2021) play critical roles in determining the amplitude and attenuation behavior of pneumatic hammer waves.

In recent years, there has been a growing body of research on the pneumatic hammer phenomenon, especially for gas-liquid two-phase issues. However, most of these studies are conducted in general pipeline systems or specific industrial scenarios, rather than gas turbine natural gas supply networks. For instance, Luo et al. (2025) conducted an experimental study and found

that in gas-liquid pipelines, the propagation of pneumatic hammer pressure waves is significantly influenced by the compressibility of the gas phase, showing significant phase delay and amplitude attenuation. As the gas-liquid ratio increases from 0.04% to 12.6%, the wave velocity of pneumatic hammer pressure waves decreases from 298 m/s to 146 m/s, which is only 21.60%–10.60% of the single-phase wave velocity. Zhang et al. (2022) conducted a simulation study on the pneumatic hammer effect in nuclear power plant pipelines in the presence of gas cavities. The results showed that the amplitude and frequency of the pipe internal pressure vary significantly with the volume ratio of the gas cavity, and a smaller gas cavity volume ratio corresponds to a lower maximum pipe internal pressure and a faster attenuation of the pressure wave. Zhao et al. (2025) further studied the pneumatic hammer effect induced by two-phase flow with large temperature differences, and established a mathematical model with compressible two-phase flow equations that takes into account the elastic deformation of the pipe cross-section to predict the pressure load of the condensate pneumatic hammer. The study showed that an increase in the flow velocity of cold pneumatic will raise the peak value of the pressure pulse; an increase in the temperature of the liquid phase will cause the peak value of the pressure to decrease; and when the pipe diameter is sufficiently small, the pneumatic hammer phenomenon will no longer occur.

On the other hand, the valve operation characteristics have been proven to be a crucial factor that determines the intensity of transient shock: rapid valve maneuvers often lead to high-amplitude pressure waves, whereas optimizing the opening and closing pattern (such as staged or gradual opening and closing) helps to reduce the peak impact and improve system stability. Lema et al. (2016) investigated the pneumatic hammer phenomenon within the pipe caused by the rapid opening of the valve and the accompanying multiphase flow characteristics. They discovered the pressure fluctuations caused by the compression and expansion waves of the fluid, as well as cavitation, gas desorption, and liquid column separation phenomena. This revealed the influence of liquid surface tension on the multiphase flow state and confirmed that gas desorption in saturated liquids can significantly reduce the transient pressure peak. Ding et al. (2024) used the SPS software to study the liquid pipeline system in the petrochemical industry and found that the influence of the valve closing duration on the pneumatic hammer effect is restricted by the pipeline length and flow rate: as the pipe length increases, the effect of extending the valve closing duration gradually weakens, while the greater the flow rate, the more obvious the effect of prolonging the time. Kaliatka et al. (2014) simulated the scenario where the pump station in the regional heating system experienced a power outage, causing the check valve to close. They analyzed the peak pipeline pressure and explored the impact of different safety valve diameters on the maximum pressure within the pipeline. Henclik (2018) studied the inhibitory

effect of elastic valves on pipeline pneumatic hammer phenomena, simulating the transient pressure and velocity variations of the fluid within the pipeline caused by the rapid closure of the valve under different stiffness conditions. It was confirmed that elastic valves can effectively regulate pneumatic hammer pressure through dynamic energy transfer and dissipation mechanisms, providing a feasible solution for scenarios where the valve closing time cannot be extended in engineering. These studies confirm that valve dynamics play a dominant role in pneumatic hammer control. However, the valve operating patterns in gas turbine natural gas systems, characterized by frequent start-stop and rapid load-following behavior, differ significantly from those in conventional industrial pipeline applications and remain insufficiently investigated.

Although previous studies have extensively investigated influencing factors such as fluid compressibility and valve operation patterns, research focusing specifically on gas turbine natural gas supply systems remains limited. Compared with liquid media, natural gas exhibits low viscosity and high compressibility, resulting in a pneumatic hammer process that is more gradual yet 148prolonged. Moreover, within the complex piping layouts of gas turbines, the transient structural response induced by pneumatic hammer, especially the dynamic behavior of supports, has not been systematically explored. This paper takes the natural gas supply pipeline system of the first 300 MW-level F-class heavy-duty gas turbine in China as the research object. Based on the combined simulation method of computational fluid dynamics and transient structural dynamics, a fluid-solid coupling model with a complete pipeline network structure is established. The propagation of pressure waves in the pipeline and the transient response characteristics under different valve opening strategies are analyzed. This provides a theoretical basis and engineering reference for optimizing valve control strategies, improving pipeline support design, and ensuring the safe and stable operation of the gas turbine.

2 Numerical model

2.1 Physical model

The research subject of this article is the natural gas supply pipeline system of a 300 MW F-class heavy-duty gas turbine. The pipeline structure consists of straight pipe sections, elbows, valves, and several hanger supports, as shown in Figure 1. The outer diameter of the pipe is 273 mm and the wall thickness is 14 mm. The length of each pipe section is shown in Table 1. To facilitate subsequent analysis, the pipe sections are numbered as shown in Figures 1a,b. The entire pipeline is made of 316L stainless steel pipes. The position L1 is the inlet point and is connected to the pre-module, while the position L15 is the outlet point and is interfaced to the gas module. Figure 1c shows the model of the pipeline and supports. Supports 1, 3, 5, 9, 10, and 11 are spring supports, support two and 6 are guide supports, support 4 is a double-pull rod rigid hanger, support 7 and 8 are sliding supports and fixed supports respectively; 12 to 15 are single-pull rod rigid hangers, and support 16 and 17 are single-pull rod spring hangers.

Due to the presence of bends and local support constraints, the local impedance differences have a significant impact on the propagation and reflection characteristics of pressure waves, and are

prone to causing local stress concentration and structural vibration. To obtain the complete flow characteristics of the fluid inside the pipeline, as well as the transient structural response of the pipeline hanger support, and the local stress-strain characteristics, a three-dimensional modelling of the complete natural gas pipeline system is carried out. The fluid domain was discretized using a multi-zone hexahedral mesh, with local refinement implemented in critical regions such as pipe bends and valve proximity. On the other hand, in the solid domain, local refinement is performed at elbows and the connection points between pipes and supports to enhance the simulation accuracy of structural responses.

2.2 Governing equations

Natural gas is a low-viscosity and highly compressible medium. Its pneumatic hammer effect is mainly influenced by the sound velocity and gas compressibility rather than viscosity dissipation. Therefore, the compressibility effect of the fluid needs to be taken into consideration in the governing equations. This paper assumes that natural gas is composed of a single component of methane (CH₄). The reason for this assumption is that in actual operating conditions, the volume fraction of methane in natural gas is usually greater than 90%, while the proportions of other components (such as ethane, propane, and nitrogen) are relatively low and have a limited impact on the overall flow properties and pneumatic hammer propagation characteristics. Therefore, to simplify the calculation and ensure the consistency of physical property parameters, methane is adopted as the research medium.

The flow field within the pipe is a compressible fluid, and its continuity equation and momentum equation are (Li et al., 2021; Liu et al., 2017; Versteeg and Malalasekera, 2010) (Equations 1–3), which are as follows:

$$\frac{\partial \rho_i}{\partial t} + \frac{\partial(\rho_i v_j)}{\partial x_j} = 0 \tag{1}$$

$$\frac{\partial(\rho_i v_j)}{\partial t} + \frac{\partial(\rho_i v_j v_i)}{\partial x_j} = -\frac{\partial p}{\partial x_i} + \frac{\partial \tau_{ij}}{\partial x_j} \tag{2}$$

$$\frac{\partial(\rho_i E)}{\partial t} + \frac{\partial[(\rho_i E + p)v_i]}{\partial x_i} = \frac{\partial(\tau_{ij} v_i)}{\partial x_j} \tag{3}$$

Among them, ρ_i and v represent fluid density and velocity, p represents fluid static pressure, and τ_{ij} represents the viscosity stress tensor.

Due to the significant non-stationary vortex structure and turbulent dissipation characteristics involved in the valve opening process, this paper adopts the SST $k-\omega$ turbulence model. It uses the $k-\omega$ model in the near-wall region and transitions to the $k-\epsilon$ model in the free-stream region. This model can accurately capture the near-wall flow and shear stress, and ensure the stability of large-scale flow simulation, making it suitable for describing the transient turbulent characteristics in natural gas pipelines. The transport equations for turbulent kinetic energy and specific dissipation rate are Equations 4, 5, which are as follows (Fan et al., 2024; Menter, 1994):

$$\frac{\partial(\rho_i k)}{\partial t} + \frac{\partial(\rho_i v_j k)}{\partial x_j} = P_k - \beta^* \rho_i \omega k + \frac{\partial}{\partial x_j} \left[(\mu + \sigma_k \mu_t) \frac{\partial k}{\partial x_j} \right] \tag{4}$$

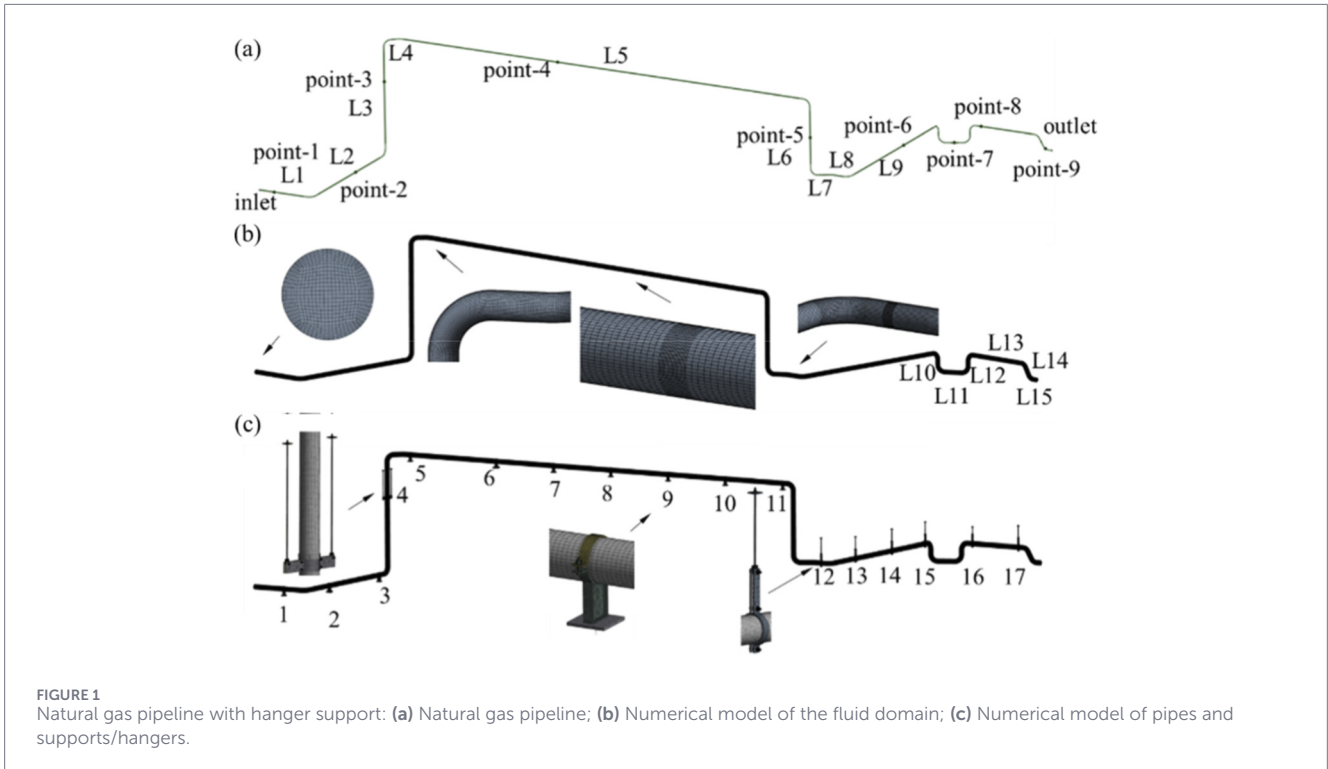


FIGURE 1 Natural gas pipeline with hanger support: (a) Natural gas pipeline; (b) Numerical model of the fluid domain; (c) Numerical model of pipes and supports/hangers.

TABLE 1 Length of the natural gas pipeline.

Position	L1	L2	L3	L4	L5
Length/mm	3540	9085	7025	990	27210
Position	L6	L7	L8	L9	L10
Length/mm	4650	1200	1161	11040	1100
Position	L11	L12	L13	L14	L15
Length/mm	1835	1100	4515	957	507

$$\frac{\partial(\rho_l \omega)}{\partial t} + \frac{\partial(\rho_l \mu_j \omega)}{\partial x_j} = \alpha \frac{\omega}{k} P_k - \beta \rho_l \omega^2 + \frac{\partial}{\partial x_j} \left[(\mu + \sigma_\omega \mu_t) \frac{\partial \omega}{\partial x_j} \right] + 2(1 - F_1) \rho_l \sigma_{\omega 2} \frac{1}{\omega} \frac{\partial k}{\partial x_j} \frac{\partial \omega}{\partial x_j} \quad (5)$$

Where k is the turbulent kinetic energy, ω is the dissipation rate, μ_t is the turbulent viscosity, P_k is the turbulent kinetic energy generation term, β^* is the turbulent kinetic energy dissipation coefficient, α is the generation term coefficient, β is the dissipation term coefficient, σ_k and σ_ω is the turbulent diffusion coefficient, $\sigma_{\omega 2}$ is the cross diffusion coefficient, F_1 and is the mixing function for controlling the near-wall region and the free-stream region in the SST model.

In the field of transient structural dynamics, the motion equation, Equation 6, based on Newton's second law (Liu, 2015) is adopted:

$$\rho_s \frac{\partial^2 d_i}{\partial t^2} + c \frac{\partial d_i}{\partial t} - \frac{\partial}{\partial x_j} \left(C_{ijkl} \frac{\partial d_k}{\partial x_l} \right) = f_i^{\text{fluid}} + f_i^{\text{boundary}} \quad (6)$$

Where ρ_s is the density of the solid material, d_i is the displacement component, c is the structural damping coefficient,

C_{ijkl} is the elastic stiffness tensor, f_i^{fluid} is the force density exerted by the fluid on the structure, and f_i^{boundary} is the density of the boundary constraint reaction force.

Due to the high elastic modulus of the natural gas pipeline and the associated supports/hangers, the structural deformation induced by valve opening remains very small under the present operating conditions. Compared with the characteristic dimensions of the flow domain, such deformation is negligible and therefore has a minimal influence on the internal flow field and pressure wave propagation. The pneumatic hammer phenomenon investigated in this study is primarily governed by fluid compressibility and valve-induced momentum variation, rather than by strong fluid-structure coupling effects. Consequently, a one-way fluid-to-structure coupling approach is adopted, which is sufficient and appropriate for capturing the transient pressure evolution in the fluid domain as well as the corresponding structural stress and deformation responses. In the calculation, data are exchanged between the fluid and solid domains at the coupling interfaces, and the following conservation principles (Yin et al., 2024) are given as Equation 7:

$$\sigma_1 n_1 = \sigma_s n_s, \varepsilon_l = \varepsilon_s \quad (7)$$

Where σ_l , σ_s and ε_l , ε_s represent the stress and strain of the fluid domain and the solid domain, respectively; n represents the normal direction of the coupling surface.

2.3 Boundary conditions

Considering the frequent load adjustments in heavy-duty gas turbines, this study investigates the extreme scenario of natural gas supply ramping from zero to maximum capacity to simulate

TABLE 2 Material parameters of Natural gas pipeline system components.

Material	316L stainless steel	Q235B structural steel
Density $\rho/\text{kg}\cdot\text{m}^{-3}$	7.98×10^3	7.85×10^3
Modulus of elasticity E/MPa	1.86×10^5	2.12×10^5
Yield strength σ_y/MPa	2.05×10^2	2.35×10^2

transient flow characteristics in the pipelines. The approach ensures structural integrity under all operational conditions. In the fluid dynamics simulation, the inlet of the main valve is set as a mass flow rate inlet, and the outlet is set as a pressure outlet boundary. The pressure value is determined as 3.8 MPa based on the rated operating condition P_n of the gas turbine. By introducing the Cv curve of the valve, the valve opening characteristic is converted into an equivalent flow variation and is applied as a time-dependent function at the inlet section. The rated operating condition is $q_n = 18.5 \text{ kg}\cdot\text{s}^{-1}$. The opening and closing rules of the valve adopt various strategies, such as linear, from fast to slow, and from slow to fast, to study the influence of different control methods on the pipeline pneumatic hammer effect.

To accurately capture the pressure fluctuations during the valve opening and closing process, the Pressure-Based Coupled algorithm is used to solve the coupling of velocity and pressure. The density, momentum, turbulent kinetic energy, and specific dissipation rate are discretized using second-order upwind schemes, and the pressure is discretized using a second-order central. The time-marching term is discretized using a first-order implicit scheme, with the time step set to $1 \times 10^{-3} \text{ s}$ to ensure the transient resolution of the pneumatic hammer wave propagation.

In the transient structural dynamics model, the two ends of the pipeline and the bases of each support and hanger are set as fixed supports, and the contact between the support hangers and the pipeline is frictional contact. The friction coefficients of the sliding support and the guiding support are set at 0.1, while those of the other connection parts are set at 0.3. The fluid-structure coupling is implemented in a one-way manner, that is, the transient pressure distribution of the fluid is mapped onto the pipe wall as the structural load input, and then the transient stress and deformation responses of the structure are solved. The time step for the structural solution is set at 0.01 s, which is coordinated with the fluid solution.

In this paper, methane is used as the research working fluid to represent natural gas, as explained previously. The thermophysical parameters of methane are directly retrieved from the built-in real-gas NIST database of Fluent, which can automatically consider its density, specific heat, viscosity, and sound speed that change with temperature and pressure, thus ensuring the accurate description of the fluid dynamic characteristics in the numerical simulation.

The material of the pipeline is 316L stainless steel, and the hanger supports are Q235B. The material parameters under standard conditions are shown in Table 2.

2.4 Model independence verification

In numerical simulations, the fineness of grid division has a significant impact on the calculation accuracy of fluid transient

characteristics and structural responses. As showed in Figure 2, this paper conducts a grid independence verification for the natural gas pipeline system, to ensure that the simulation results are independent of the grid size.

For the fluid domain, five different meshes were established, with the number of elements ranging from 1300×10^3 to 3400×10^3 . Since the pneumatic hammer effect is manifested as high-frequency pressure fluctuations caused by the opening and closing of the valve, the maximum pressure P_{max} under the condition of rapid valve opening was selected as the criterion for the independence of the fluid domain mesh. The results show that when the mesh size increased from 2.34 million to 3.40 million, the maximum pressure difference measured inside the pipeline was less than 1%, indicating that a medium-sized mesh can ensure the accurate capture of the pressure wave propagation law.

For the solid domain, five mesh schemes were also established, with the number of elements ranging from approximately 1300×10^3 to 3400×10^3 . Local mesh refinement was carried out near the bends, valves, and connection points of the hanger support. Since the focus of the project is on the transient structural response under the pneumatic hammer effect, the maximum equivalent stress $\sigma_{eq,max}$ of the entire pipeline was selected as the criterion. The calculation results show that when the number of nodes increased from 2.33 million to 3.33 million, the variation of the equivalent stress was less than 1%. Therefore, medium-sized nodes can already meet the calculation accuracy requirements.

Furthermore, to ensure the temporal resolution of the transient process, this paper verified the independence of time steps in the fluid and structural calculations. The results showed that in the fluid calculation, when the time step was reduced from $1 \times 10^{-3} \text{ s}$ to $1 \times 10^{-4} \text{ s}$, the maximum pressure variation amplitude was less than 1%; in the structural response, when the time step was reduced from $1 \times 10^{-2} \text{ s}$ to $5 \times 10^{-3} \text{ s}$, the maximum equivalent stress was less than 1%. This indicates that a time step of $1 \times 10^{-3} \text{ s}$ is sufficient to capture the characteristics of transient pneumatic hammer fluctuations, while a time step of $1 \times 10^{-2} \text{ s}$ meets the requirements for structural response calculations. In addition to numerical convergence, the predicted transient pressure wave propagation shows physically consistent behavior for pneumatic hammer in compressible gas pipelines. The pressure peak variations under different valve opening strategies are smooth and monotonic, without spurious numerical oscillations.

Taking into account both computational accuracy and efficiency, this paper finally selects a medium-sized grid scheme with approximately 2.34 million elements for the fluid domain and approximately 2.33 million nodes for the solid domain. The time step for fluid calculations is fixed at $1 \times 10^{-3} \text{ s}$, and the time step for solid domain calculations is fixed at $1 \times 10^{-2} \text{ s}$, which will be used for the subsequent transient fluid-solid coupling calculations.

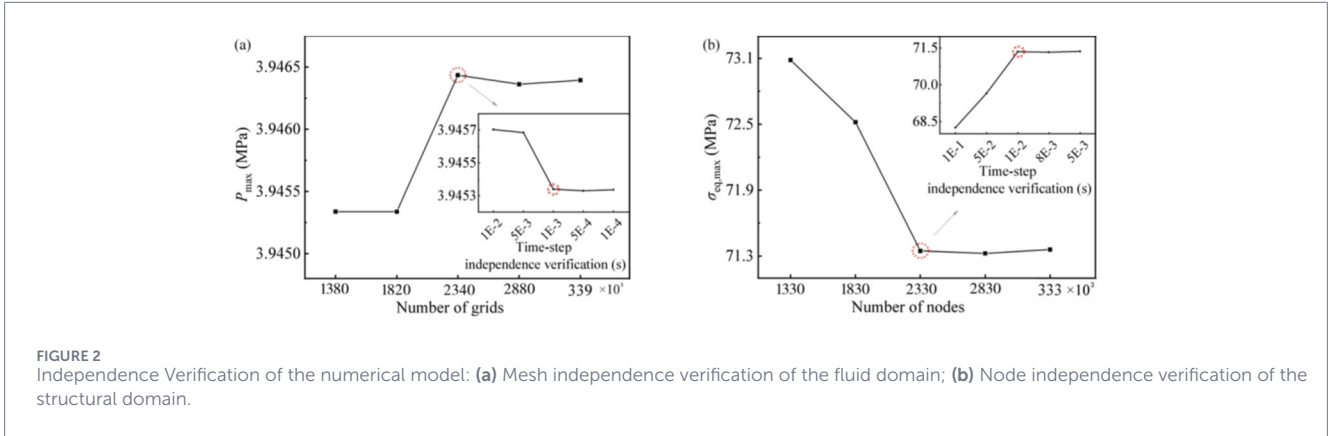


TABLE 3 Valve flow characteristics.

Fisher valve Stroke/deg	0	15	20	30	40	50	60	70	80	90
SRV position/%	0	17.78	24.06	36.82	49.52	61.81	73.33	83.81	92.98	100
$q/\text{kg}\cdot\text{s}^{-1}$	0	3.29	4.45	6.81	9.16	11.43	13.57	15.41	17.20	18.5

3 Result analysis and discussions

3.1 Fluid flow characteristics

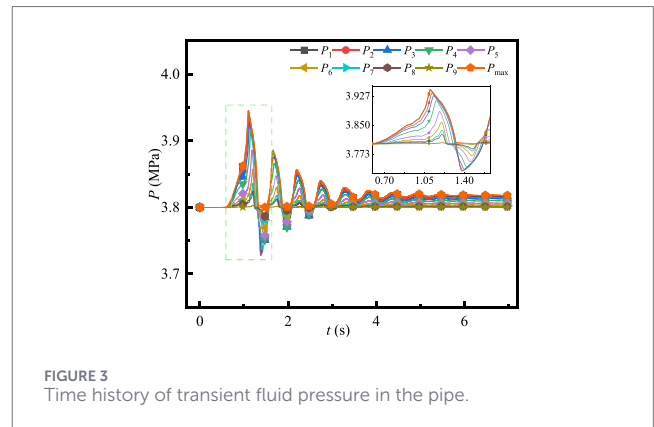
3.1.1 Flow characteristics within the pipe

Based on the characteristics of the Woodward 8-inch SS-260 Ga Stop/Ratio Valve, its flow characteristics are shown in Table 3.

Let the time when the valve starts to be opened be t_0 , and the time when it is fully opened be t_c . Then the opening time Δt is the difference between the two. According to the operational requirements of the system, Δt is within the range of 0.2 s–1 s. The flow field is initialized with the rated working condition of 3.8 MPa as the initial pressure inside the pipe. At $t_0 = 0.5$ s, the valve is controlled to be opened and the opening degree increases at a linear rate. It is fully opened at $t_c = 1.1$ s. During this process, the inlet mass flow rate q gradually increases from 0 to the rated flow rate $q_n = 18.5$ kg/s and remains stable afterwards.

The pressure variations at each monitoring point are shown in Figure 3. As the valve is opened, the pressure in the pipeline undergoes a complete evolution process from intense fluctuations to gradual stability. Specifically, at the moment the valve is just opened (t_0), no instantaneous sharp peak of overpressure is generated. Instead, the pressure initially rises at a moderate rate and reaches the maximum positive peak near the complete opening moment (t_c); then immediately followed by a brief negative undershoot. This is succeeded by multi-cycle, progressively decaying oscillations that eventually stabilize.

This temporal characteristic indicates that the compressibility of natural gas causes the local fluid to be compressed during the valve opening process and form a positive pressure wave, which then propagates along the pipeline at the speed of sound. Under linear valve opening conditions, the valve disc opening degree increases linearly and continuously rather than suddenly. Therefore,



the compression effect of the gas in the pipe accumulates gradually, resulting in a gradual increase in pressure. No sudden and intense high pressure was observed near t_0 .

As the valve is gradually opened, the mass flow rate at the inlet continues to increase. Under the combined effect of mass inertia in the pipe and local resistance, the compression wave intensifies continuously and reaches its peak at the maximum flow rate. The subsequent obvious negative peak indicates that a rarefaction process occurs after the compression wave. On one hand, when the flow approaches the rated flow rate, the local flow changes from a restricted state to a more unobstructed state, and the sudden change in flow velocity forms a refraction wave front, resulting in a short-term negative peak. On the other hand, the interference between the reflected wave at the far end (especially at the bend or constraint point) and the original compression wave may also cause a local negative amplitude waveform. In Figure 3, the negative peak follows the positive peak, indicating that the compression and refraction waves are closely coupled in time.

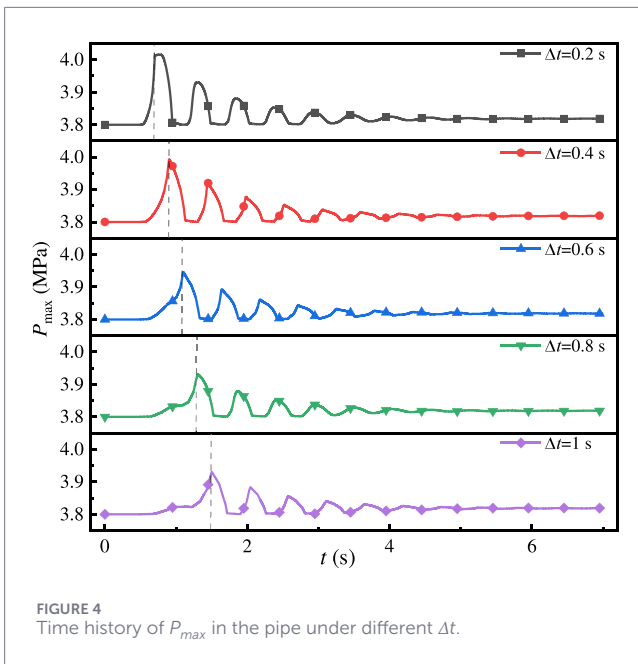


FIGURE 4 Time history of P_{max} in the pipe under different Δt .

TABLE 4 Maximum transient fluid pressure in the pipe under different Δt .

$\Delta t/s$	0.2	0.4	0.6	0.8	1
P_{max}/MPa	4.016	3.992	3.945	3.931	3.930
Error bar/MPa	0.001	0.001	0.001	0.001	0.001

3.4% over 3.8 MPa). This result indicates that the shorter the opening time of the valve, the greater the transient overpressure, and the more intense the pressure fluctuation. The fundamental reason lies in the fact that the valve’s action rate directly affects the rate of change of fluid momentum.

A further analysis of Figure 4 reveals that the time history of the maximum pressure under different valve opening times not only differs in peak magnitude but also has significantly different peak shapes. When $\Delta t = 0.2$ s, the pressure rises rapidly in the opening stage in a quasi-linear trend. After reaching the peak, the pressure amplitude does not drop immediately. Instead, it exhibits a brief ‘flat-topped’ feature, meaning the peak area presents a smooth and rounded shape. This indicates that during the rapid valve opening process, the rate of change in gas momentum is extremely high, and the local pressure remains at a high level after reaching the peak. At this time, the flow area of the valve rapidly expands, and the gas undergoes short-term compression and expansion simultaneously near the valve opening. The local static pressure and dynamic pressure alternate and balance each other out, causing the pressure curve to experience a short-term stagnation during the peak stage.

When the valve opening time is extended to 0.4 s or longer, the peak shape transforms into a sharp one. Once the peak is reached, the pressure rapidly drops. This indicates that the pressure energy release is smoother at this time, and the system response is more gentle. At the same time, it can be observed that under the condition of $\Delta t = 0.6$ s, the pressure growth rate during valve opening shows a significant slowdown; while at $\Delta t = 0.8$ s, this phenomenon is more obvious; and at $\Delta t = 1$ s, there even appears a nearly horizontal pressure interval. The reason for this is as follows: although the valve opening degree increases linearly over time, the valve flow coefficient has a non-linear relationship with the opening degree, resulting in a ‘slow start followed by a rapid increase’ in flow rate. Therefore, during the initial stage of valve opening, the gas flow increases slowly and the pressure change is limited; in the latter half of the opening process, the flow increases rapidly, the momentum surges, the pressure increase rate accelerates again, and reaches its peak when the valve is fully opened.

In summary, the opening time of the valve determines the variation pattern of the flow acceleration and the rate of energy release in the system: when Δt is small, that is, when the valve is opened quickly, the sudden change in fluid momentum is significant, and the local compression energy accumulates rapidly within a short period of time to form a high peak, which then decays rapidly; when Δt is large, that is, when the valve is opened slowly, the energy is gradually transferred and buffered by the compressible effect, forming a peak-shaped pressure curve but with a lower peak value.

Therefore, although the compressibility of the gas medium results in significantly lower pneumatic hammer peak values compared to liquid systems, appropriately extending the valve opening time remains an important measure for suppressing

The subsequently observed alternating positive and negative oscillations and the gradually decreasing peak variations reflect the multiple reflections of the pressure waves in the pipeline, accompanied by energy dissipation along the way. The compressibility of the gas makes a smoother waveform and slower attenuation, so obvious fluctuations remain for several cycles until the energy is completely dissipated before a steady state is reached.

Furthermore, from Figure 3, it can also be observed that there is a significant time-phase lag and amplitude attenuation in the pressure peaks at different measurement points. This phase delay of several tens of milliseconds between different measurement points is consistent with the propagation of a pressure wave at the speed of sound (the speed of sound of methane under the conditions of 3.8 MPa and 200 °C is approximately 510 m/s).

From the above, it can be seen that under the linear valve-opening condition, the pneumatic hammer phenomenon exhibits the characteristics of ‘no initial peak, dominated by a positive peak close to the end of the opening, followed by a negative peak and accompanied by long-period attenuation oscillations’ in the gas transient response.

3.1.2 The influence of valve opening duration

The influence of the valve opening duration on the pneumatic hammer effect is tested by setting the valve opening time Δt to 0.2 s, 0.4 s, 0.6 s, 0.8 s, and 1 s. The maximum pressure changes in the pipeline under each condition are shown in Figure 4, and the maximum pressure data are presented in Table 4.

From Figure 4 and Table 4, it can be observed that as the opening time of the valve increases, the maximum pressure in the pipe shows a significant decreasing trend. When $\Delta t = 0.2$ s, the pressure peak reaches 4.016 MPa, resulting in an overpressure of approximately 0.216 MPa (about 5.7%) compared to the rated pressure of 3.8 MPa. As Δt is extended to 1.0 s, the maximum pressure drops to 3.930 MPa, with an overpressure amplitude being only 0.130 MPa (about

transient overpressure and reducing reflection superposition in natural gas pipelines.

3.1.3 The impact of valve opening characteristics

To study the influence of valve opening patterns on the pneumatically hammer effect in natural gas pipelines, the valve opening strategy influencing factor m is introduced. The maximum valve opening is θ_n . Then, within the time interval from t_0 to t_c , the relationship between valve opening θ and time t is Equation 8, which is as follows:

$$\theta = \theta_n \left(\frac{t - t_0}{t_c - t_0} \right)^m \tag{8}$$

When $m = 1$, it indicates that the valve opening increases at a linear rate; when $m < 1$, it is a ‘from fast to slow’ type of valve opening; when $m > 1$, it is a ‘from slow to fast’ type of valve opening. Setting $t_0 = 0.5$ s, $\Delta t = 0.6$ s, and letting m be 0.1, 0.2, 0.25, 0.5, 1, and 2, respectively, the flow and pressure responses under different valve opening strategies are simulated.

Figure 5 shows the variation curves of the valve inlet flow under each strategy. As shown in Figure 5, the valve opening strategy factor m significantly alters the growth pattern of the inlet mass flow rate. When $m = 1$, the flow curve most directly reflects the relationship between the valve characteristics and the opening degree, presenting a typical ‘from slow to fast’ feature, which is caused by the non-linear correspondence between the valve flow coefficient and the opening degree. When $m < 0.5$, the flow curve exhibits a distinct ‘from slow to fast’ characteristic: the flow area suddenly increases at the moment the valve is opened, and the inlet flow rate rises sharply in a short period of time. However, the rate of increase gradually slows down subsequently, and the curve gradually turns into a nearly linear trend, reaching the rated flow at t_c . As m increases, the curve shape changes. For example, when $m = 0.5$, it presents two linear segments with different slopes, being slow at the beginning and then fast at the end. When $m > 1$, the ‘from slow to fast’ valve opening strategy, combined with the valve’s own ‘from slow to fast’ flow characteristic, results in an extremely gradual initial increase in flow rate, followed by a sharp rise in the later stage. The slope of the curve increases sharply, presenting the characteristic of ‘slow start, fast rise’. It can be seen that this nonlinear flow change controlled by m directly determines the growth rate of the gas momentum within the pipe, and is a key factor affecting the shape of the pressure wave.

Figure 6 shows the corresponding maximum pressure changes in the pipe, and Table 5 gives the maximum pressure results under each condition. The pressure changes shown in Figure 6 can further reveal the transient response characteristics under different valve opening strategies. When $m < 1$, the maximum pressure curve exhibits a distinct double-peak structure within the time interval from t_0 to t_c : near t_0 , the pressure experiences a nearly vertical sudden rise, then increases and reaches the first peak, followed by a brief decrease. As the valve is further opened and the flow rate increases, the pressure reaches the peak at t_c . Among them, the initial jump with $m = 0.1$ is the most intense, and the first peak is also the highest, being higher than the peak when t_c is reached; the jump with $m = 0.2$ is weaker, and the first peak drops but remains higher than the S peak; while when $m = 0.25$, the two peaks are close. This is because at the beginning of opening the valve, the valve

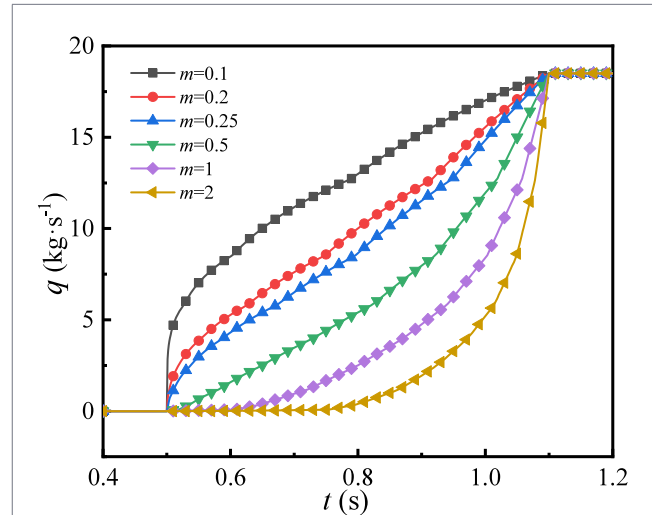


FIGURE 5 Time history of inlet mass flow rate under different m .

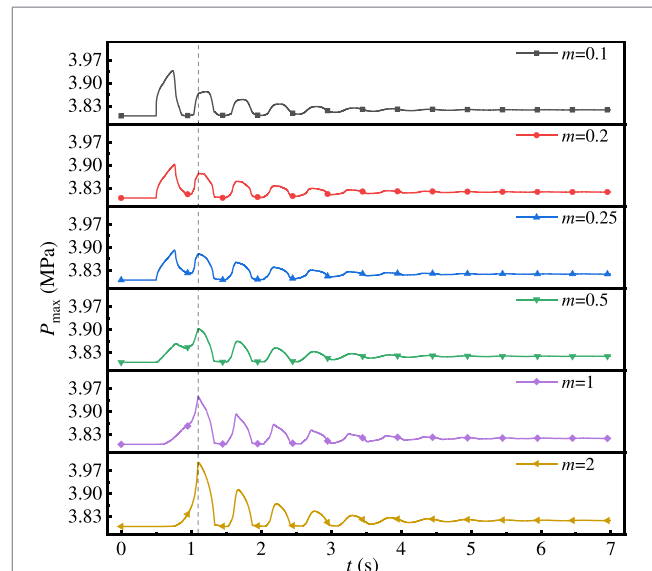


FIGURE 6 Time history of maximum transient fluid pressure in the pipe under different m .

TABLE 5 Maximum transient fluid pressure in the pipe under different m .

m	0.1	0.2	0.25	0.5	1	2
P_{max}/MPa	3.938	3.903	3.891	3.903	3.945	3.995
Error bar/MPa	0.001	0.001	0.001	0.001	0.001	0.001

disc opens rapidly for a short period of time, causing a significant compression wave; subsequently, the opening degree enters a slow increase stage, the flow acceleration decreases, and the pressure briefly drops; later, as the flow increases again, a compression wave forms and superimposes, resulting in a double-peak pattern.

When $m = 0.5$, the initial rising stage of the pressure gradually becomes smoother, without any obvious jumps. Instead, it rises approximately linearly, and its first peak is lower than the peak at t_c . When $m \geq 1$, the pressure curve presents a single-peak structure: the system shows a monotonic increase throughout the valve opening stage. When $m = 1$, the pressure pauses slightly in the middle period before accelerating again and reaching the peak at t_c ; when $m = 2$, the pressure initially rises more smoothly, then climbs rapidly in the later stage, and finally forms a higher main peak.

From Table 5, it can be seen that the maximum pressure varies between 3.891 MPa and 3.995 MPa, with a peak difference of approximately 0.1 MPa. The overall trend is that the maximum pressure first decreases and then increases as m increases: when m is too small (such as $m = 0.1, 0.2$), the short-term rapid opening of the valve disc leads to a significant initial compression wave, resulting in a double peak and the first peak being larger; while when m is larger (such as $m = 1, 2$), it presents a single peak shape, but the superposition of the valve flow coefficient and the rapid increase in opening degree makes the pressure at t_c higher. From the perspective of flow characteristics, the ‘first fast then slow’ type valve opening ($m < 1$) enables the system to quickly establish a flow channel in the initial stage. However, when m is too small, a pressure jump may occur. But in the later stage, the growth of the flow rate slows down, and the rate of momentum change decreases, which in turn allows the compression wave to be gradually released during propagation. On the contrary, the ‘first slow then fast’ type ($m > 1$) is due to the restricted flow in the early stage and the accumulation of momentum. In the later stage, the sudden release of a large flow rate causes the gas compression wave to be concentratedly superimposed, resulting in a higher main peak pressure.

To further illustrate that a valve opening strategy with $m = 0.25$ results in the smallest air hammer strength, it is necessary to analyze in terms of fluid momentum change and gas compressibility. The pneumatic hammer phenomenon in compressible gas pipelines is primarily governed by the temporal rate of change of fluid momentum rather than by the absolute flow rate. The valve opening parameter m directly controls the growth pattern of the mass flow rate, thereby regulating the distribution of momentum input during the opening process. When m is small, the valve introduces a relatively large effective flow area at the early stage of opening, resulting in a rapid increase in mass flow rate and a highly concentrated gas compression process. This causes a strong local pressure rise and a higher pneumatic hammer peak. In contrast, when m is large, the flow rate increases slowly at the beginning but accelerates sharply near the fully open position, leading to compression wave superposition and amplified pressure peaks in the later stage. For $m = 0.25$, the mass flow rate increases in a more evenly distributed manner throughout the valve opening duration. This strategy effectively avoids abrupt flow acceleration in the early stage and suppresses excessive pressure accumulation in the later stage. As a result, the compressibility of natural gas can provide sufficient buffering to dissipate pressure disturbances over time, leading to the lowest peak pneumatic hammer pressure among all investigated cases. Therefore, the optimal performance of $m = 0.25$ can be attributed to its ability to balance the temporal distribution of fluid momentum.

In conclusion, the variation pattern of valve opening has a significant impact on the pneumatic hammer effect in natural gas

pipelines. The ‘from slow to fast’ type of valve opening ($m < 1$) results in a sudden increase in flow rate in the early stage but a gradual release in the later stage, forming a double-peak structure, with overall overpressure being relatively low; the linear valve opening ($m = 1$) has a stable response and moderate pressure changes; the ‘from slow to fast’ type of valve opening ($m > 1$) generates a single peak of high pressure, and the system’s transient response is the strongest. Among them, when $m = 0.25$, the two peaks are close and the energy distribution is balanced, indicating that the system has reached a more optimal dynamic response state. It can both start quickly and alleviate the concentrated superposition of gas compression waves at t_c . Therefore, for the gas turbine supply system with valve characteristics of ‘from slow to fast’, it is recommended to adopt the valve control strategy of ‘fast start and slow opening’ to disperse momentum changes, reduce pressure peaks, and improve the transient safety of the pipeline.

3.2 Structural response analysis

3.2.1 Dynamic response characteristics of structure

The pressure fluctuations within the pipeline caused by the opening of the valve exert dynamic loads on the structure of the natural gas pipeline, thereby inducing the dynamic response of the structure. To accurately simulate this transient process, this paper establishes a fluid-solid coupling dynamic model of the entire natural gas supply system, comprising the pipeline and its support structures. In the coupled analysis, the static pressure load before valve opening is first applied to simulate the initial steady state of the system; subsequently, under each valve opening condition, the transient pressure distribution calculated from the flow field is applied to the inner wall of the pipeline to analyze the excitation effect of the pressure waves caused by the valve opening on the pipeline and the hanger support.

The structural response results under the condition of $m = 1$ and $\Delta t = 0.6$ s are shown in Figures 7–11. Figure 7 presents the time history curve of the total deformation of the system and the pipeline. It can be seen that the total deformation d during the valve opening process shows obvious oscillations, and the total deformation curves of the system and the pipeline overlap, indicating that the maximum deformation occurs on the pipeline. When the valve is not opened, the static deformation of the system under the action of its own weight is 18.81 mm, which is determined jointly by the elasticity of the pipeline and the support stiffness.

At the beginning of valve opening (t_0), the propagation of the pressure wave led to a slight decrease in the total deformation of the pipeline, resulting in the formation of the first negative peak (18.40 mm). Subsequently, as the flow rate gradually increased, the pipeline’s compression deformation intensified, and the deformation increased and reached the first positive peak (19.10 mm) within a short period of time. This moment corresponded to the first peak of fluid pressure, with an increment of 0.29 mm relative to the initial static deformation. Subsequently, as the pressure wave propagated further downstream and the local density reduction effect occurred, the deformation decreased to the S negative peak (17.67 mm), and then rose to the positive peak (22.36 mm) at $t = 1.4$ s. This peak corresponded to the moment when the maximum

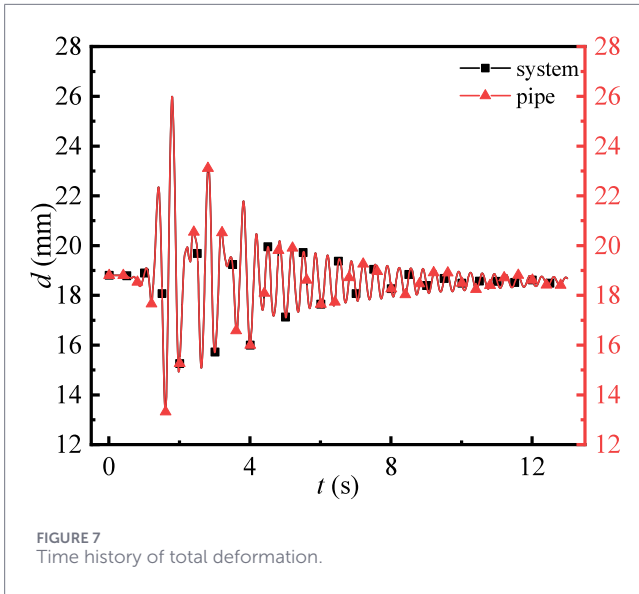


FIGURE 7 Time history of total deformation.

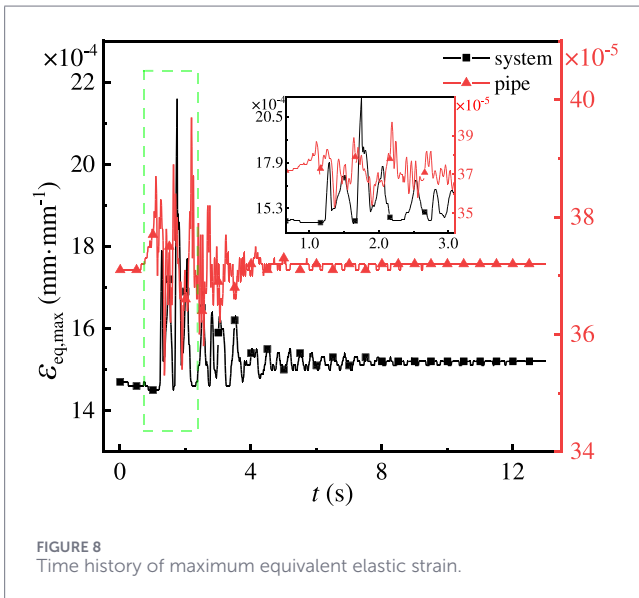


FIGURE 8 Time history of maximum equivalent elastic strain.

negative pressure was present in Figure 3. After that, affected by multiple reflections and interference, the deformation of the pipeline continued to fluctuate. It first dropped to the third and deepest negative peak (13.32 mm), and then rose to the maximum positive peak (25.97 mm). During the subsequent fluctuations, the system deformation gradually decayed and eventually tended towards a new steady-state equilibrium.

This evolution of pipeline deformation is closely related to the propagation, reflection, and interference of pressure waves of gas. In the initial stage of opening the valve, the pressure wave spreads smoothly, causing a relatively weak structural response; as the flow rate gradually increases, the accumulation of compression waves leads to an increase in the deformation amplitude. Subsequently, the alternating positive and negative peaks reflect the compression and rarefaction process of the pressure waves, and the eventual

dissipation of wave energy results in the system returning to a stable state.

Figures 8, 9 show the time history diagram of the maximum equivalent elastic strain and the contour plot of the total deformation amount, respectively. As can be seen from the figures, the system shows a relatively obvious deformation between hanger supports 9 to 13. Among them, the section from support and hanger 9–11 has a displacement direction mainly in the direction of gravity with some fluid flow direction, while the section from support and hanger 11 to hanger 13 has a displacement direction mainly along the fluid flow direction. The maximum total deformation (25.97 mm) occurs on the pipeline, but it is the comprehensive superposition of the small deformations throughout the system. From Figure 8, it can be seen that the maximum equivalent elastic strain $\epsilon_{eq,max}$ of the pipeline is only $3.97 \times 10^{-4} \text{ mm}\cdot\text{mm}^{-1}$, which belongs to a very small elastic deformation category. This indicates that the feedback effect of the structure on the fluid can be ignored, and also verifies the rationality of the unidirectional coupling assumption.

Figure 10 shows the maximum equivalent stress variation of the pipeline and the system during the valve opening process. Initially, as the valve is opened, the maximum equivalent stress increases with the increase in pressure and reaches the first peak at t_c . Subsequently, the stress variation trends of the system and the pipeline begin to diverge. The maximum equivalent stress on the pipeline shows high-frequency and intense fluctuation features, which are caused by the direct application of transient pressure waves of the fluid and their reflections and interference.

Figure 11 shows the stress contour map of the system at $t = 1.74 \text{ s}$. It can be seen that the maximum equivalent stress occurs at the single-hole pad plate of the support 13, reaching 409.41 MPa, mainly due to stress concentration. The high-stress region is located at the edge of the circular hole of the pad plate, which represents a typical geometric discontinuity-induced local stress concentration. The affected area is extremely limited and does not involve the pipeline body or the main load-bearing components of the support system. The reflection and interference of the pressure waves gradually filter out after passing through components such as pipes, hangers, and booms. Therefore, they are more regularly displayed in Figure 10. The stress concentration also occurs at the edge of the hanger, with a value of 265.77 MPa. Although this value slightly exceeds the yield strength of Q235B structural steel (235 MPa), the high-stress zone is confined to a very small region near the lifting ring boundary and does not propagate into the surrounding structural members. From an engineering design perspective, such localized stress concentrations can be effectively mitigated through local reinforcement measures, for example, by increasing the thickness or stiffness of the lifting ring. Both stress values exceed the yield strength of Q235B structural steel, but due to the relatively small concentrated range, together with the fact that these regions are not located in the primary load-bearing paths of the pipeline system, combined with the maximum equivalent elastic strain of the system being $2.15 \times 10^{-3} \text{ mm}\cdot\text{mm}^{-1}$, it can be considered that it does not pose a threat to the overall structural strength.

In addition, larger equivalent stresses are also present at the bends and supports where significant deformation occurs, especially at the positions of the cables of hangers 12 and 13. This indicates that these areas play a crucial role in the system's support. To enhance the safety margin of the system, it is recommended to focus

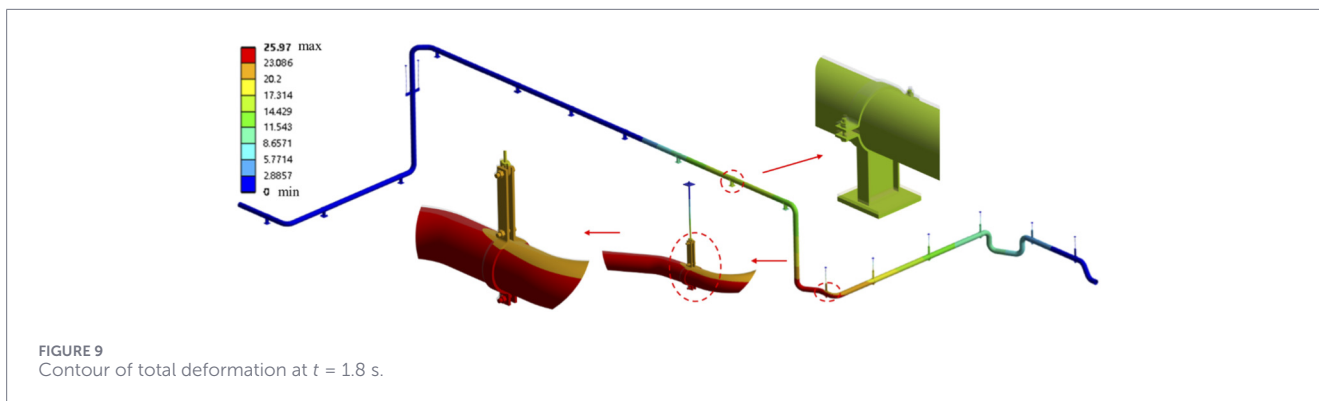


FIGURE 9 Contour of total deformation at $t = 1.8$ s.

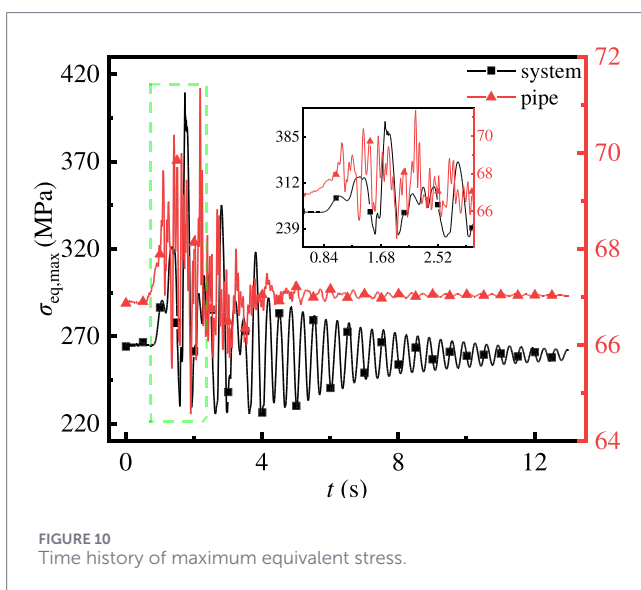


FIGURE 10 Time history of maximum equivalent stress.

on strengthening the stiffness and implementing reinforcement measures in these areas during subsequent design and maintenance.

To further verify the structural safety, this paper conducted strength checks on the maximum equivalent stress of the pipelines and supports/hangers during both the steady-state and transient phases. The local stress concentration areas of the single-hole pad plates and the lifting rings were excluded from the assessment, and the focus was on the maximum stress values in other parts of the system. The strength check results are shown in Table 6. The results indicate that the stress in the main load-bearing areas of the system is all below the allowable value of the material, meeting the structural strength requirements.

3.2.2 The impact of opening valve time

In the aforementioned analysis, it can be observed that if the maximum equivalent stress is directly used to draw the time history diagram, the results are often strongly influenced by local stress concentration. Especially at the connection points of single-hole pad plates and hangers, local peaks will mask the overall response pattern. To overcome this problem, in the subsequent steps, the

system will be divided into the pipeline part and the support-hanging part, and the average equivalent stress will be used to draw the time history diagram separately. This will weaken the interference of local concentrated effects and more clearly reveal the overall dynamic response pattern of the system under different valve opening strategies.

After coupling the fluid pressure results with different valve opening times to the structural field, the obtained response results are shown in Figures 12, 13. As can be seen from the figures, the average equivalent stress of the pipeline is basically in phase with the fluid pressure; that is, the pressure wave is transmitted to the pipe wall and immediately triggers the corresponding stress response, which fluctuates synchronously with the pressure oscillation. Due to the use of the average value, the curves are smoother compared to the local maximum stress, and can clearly reflect the periodic oscillation and energy attenuation laws caused by the pressure wave. In contrast, the average equivalent stress of the support and hanger has a lag of approximately 0.2 s. After the first peak, the stress response of the support and hanger gradually became influenced by the transmitted loads from the pipeline. During different stages, there were phenomena of stress reduction or amplification, and the oscillation frequency was significantly higher than that of the pipeline. As can be seen from Figure 13, the maximum stress peak of the support and hanger occurs after the first peak, and the oscillation is more intense than that of the pipeline. And from the comparison of stress amplitudes, it can be known that when $\Delta t = 0.2$ s, the average stress of the pipeline rises from approximately 30.79 MPa–31.94 MPa, with an increment of 1.15 MPa; while the average stress of the support and hanger increases from 12.09 MPa to 16.05 MPa, with an increment of 3.96 MPa. Thus, as a key component for load transmission and constraint, the support and hanger experiences more concentrated force and is prone to dynamic amplification effects.

The phase relationship between internal pressure fluctuations and structural response provides further insight into the dynamic behavior of the pipeline-support system. This phenomenon can be explained by the difference in dynamic characteristics between the pipe body and the support system. The pipe itself has relatively high axial and circumferential stiffness, allowing it to respond rapidly to pressure-induced loading. In contrast, the hanger supports can be regarded as elastic structures with finite stiffness and damping, whose transient response follows the behavior of a second-order dynamic system. Under excitation

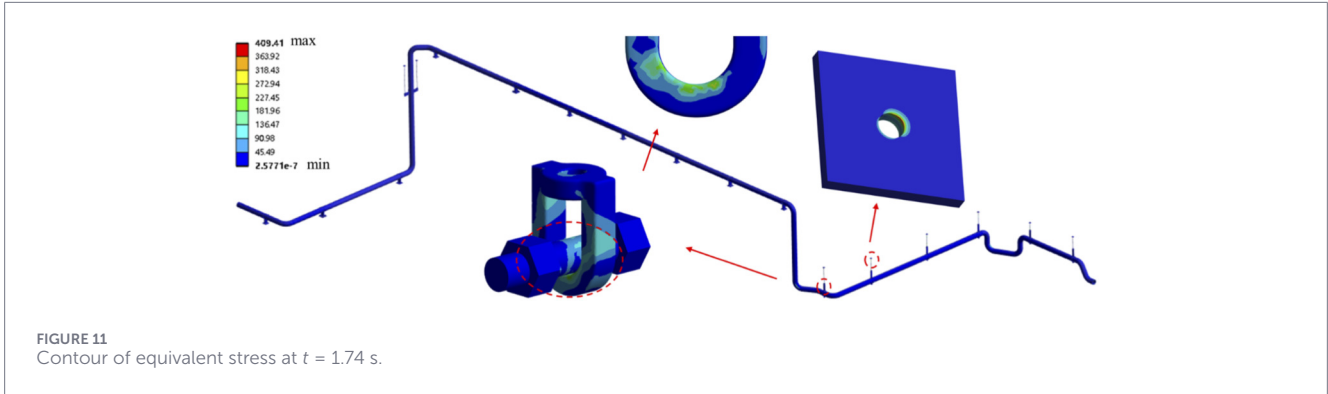


FIGURE 11 Contour of equivalent stress at $t = 1.74$ s.

TABLE 6 Strength verification results of main load-bearing regions in the system.

Position	Maximum equivalent stress $\sigma_{eq,max}$ /MPa		Material allowable stress $[\sigma]$ /MPa	Check result
	Before valve opening	After valve opening		
Pipe	66.91	71.35	205	Compliant
Hanger support	100.17	102.44	235	Compliant

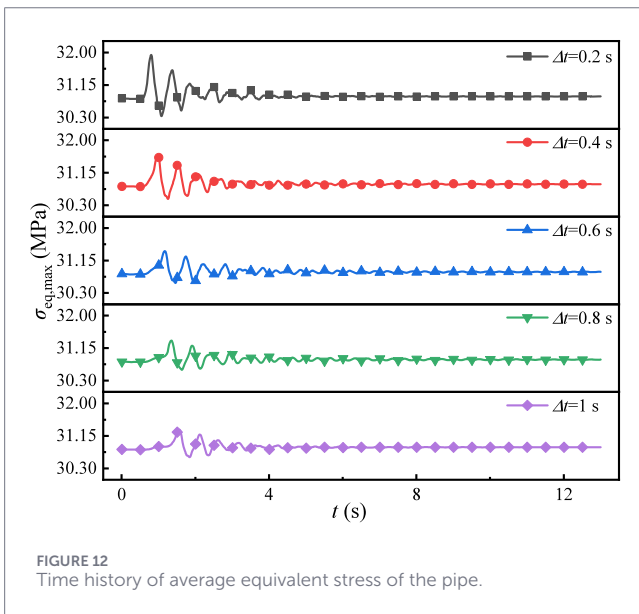


FIGURE 12 Time history of average equivalent stress of the pipe.

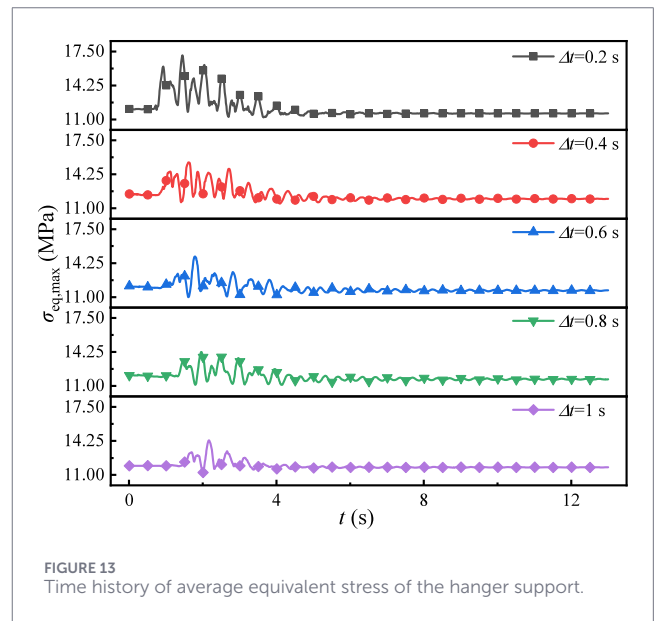


FIGURE 13 Time history of average equivalent stress of the hanger support.

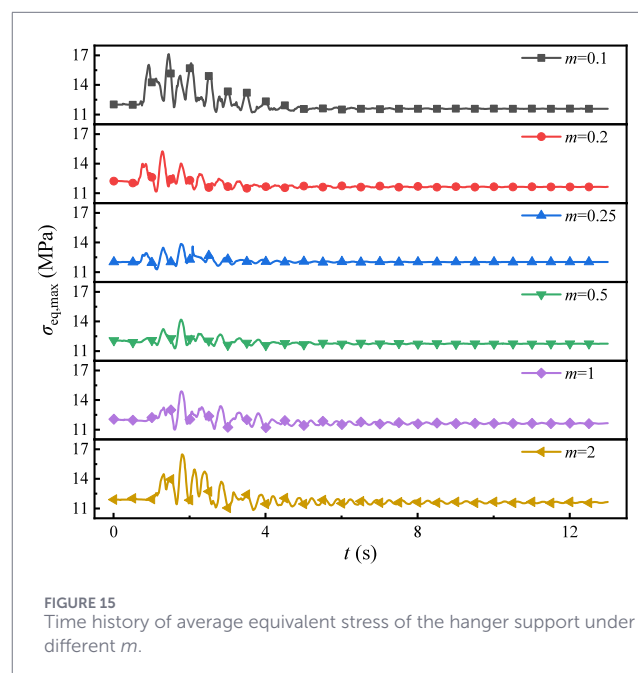
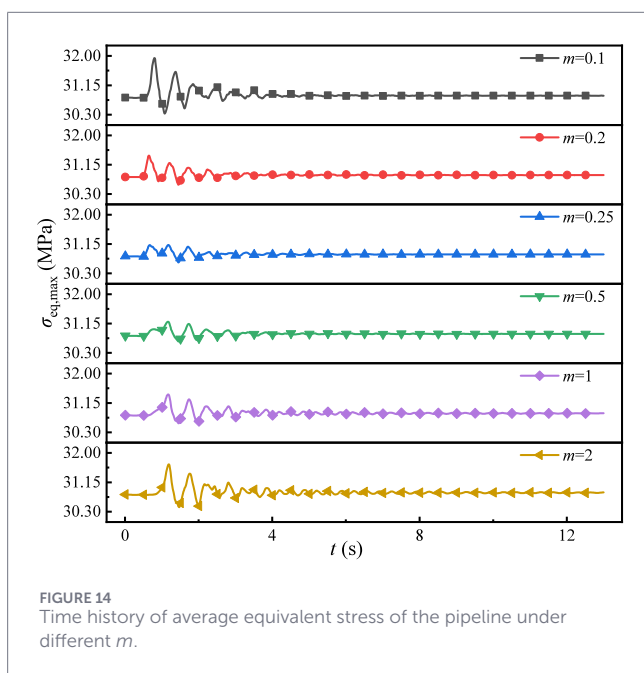
induced by valve opening, the structural response of the supports inevitably lags behind the pressure excitation. Moreover, the observed phase lag is accompanied by a certain degree of dynamic amplification, indicating that the supports actively participate in the transient energy storage and release process. This highlights that hanger supports should not be treated as purely static components when analyzing pneumatic hammer effects. From an engineering perspective, this finding implies that the natural frequencies of support systems should be carefully designed to avoid resonance with pressure wave frequencies induced by valve operations. Additionally, increasing support stiffness, introducing additional damping, or optimizing support configurations can effectively reduce phase lag and transient stress amplification,

thereby enhancing the safety and reliability of gas turbine natural gas pipeline systems.

Further analysis of the results under different valve opening times reveals that the valve opening rate has a significant impact on the structural response. For the pipeline section, its stress can quickly respond to changes in fluid pressure, and the average equivalent stress time history is almost consistent with the pressure curve inside the pipe. Under short valve opening times, due to the nonlinear relationship between the valve flow coefficient and the opening degree of 'from slow to fast', the flow increases sharply in the latter half, resulting in the most significant stress peak near t_c . As the valve opening time increases, the rising rate of pressure wave gradually

TABLE 7 Strength verification results of main load-bearing regions under different Δt .

$\Delta t/s$	Position	Maximum equivalent stress $\sigma_{eq,max}/MPa$		Material allowable stress $[\sigma]/MPa$	Check result
		Before valve opening	After valve opening		
0.2	Pipe	66.91	80.26	205	Compliant
	Hanger support	95.17	111.92	235	Compliant
0.4	Pipe	66.91	74.53	205	Compliant
	Hanger support	95.16	104.24	235	Compliant
0.6	Pipe	66.91	71.35	205	Compliant
	Hanger support	95.17	102.44	235	Compliant
0.8	Pipe	66.90	69.89	205	Compliant
	Hanger support	95.17	101.85	235	Compliant
1	Pipe	66.90	69.87	205	Compliant
	Hanger support	95.17	100.25	235	Compliant



slows down, the fluid momentum change is smoothed and dispersed in time, and the structural loading amplitude decreases accordingly, with the peak stress significantly reduced. For the support and hanger part, due to the lagging characteristic, the valve opening time and the peak value of the average equivalent stress are not in a strong linear relationship. In general, under a short valve opening time, the fluid energy is concentratedly released, and the energy interference caused by the phase lag accumulates, resulting in higher stress peaks and more intense oscillations in the support and hanger; while when the valve opening time is prolonged, the release process of the system pressure wave energy becomes more gradual, the high-frequency response of the support and hanger is suppressed, and the average stress peak and oscillation amplitude are significantly reduced, making the overall dynamic response more stable.

In conclusion, extending the valve opening time not only reduces the peak direct pressure on the pipeline but also effectively mitigates the dynamic amplification effect of the hanger support, thereby improving the structural safety of the natural gas pipeline system. The strength verification results of the main structural components of the system are listed in Table 7. The results show that the equivalent stress of all the main load-bearing components is lower than the allowable stress of the material, and the structural safety meets the requirements.

3.2.3 The impact of valve opening characteristics

The simulated gas pressure with different valve opening characteristics was coupled to the structure, and the pipeline's

TABLE 8 Strength verification results of main load-bearing regions under different m .

m	Position	Maximum equivalent stress $\sigma_{eq,max}$ /MPa		Material allowable stress $[\sigma]$ /MPa	Check result
		Before valve opening	Before valve opening		
0.1	Pipe	66.90	71.26	205	Compliant
	Hanger support	95.17	104.19	235	Compliant
0.2	Pipe	66.91	70.35	205	Compliant
	Hanger support	95.18	100.95	235	Compliant
0.25	Pipe	66.90	68.40	205	Compliant
	Hanger support	95.17	100.78	235	Compliant
0.5	Pipe	66.90	68.90	205	Compliant
	Hanger support	95.18	102.04	235	Compliant
1	Pipe	66.91	71.35	205	Compliant
	Hanger support	95.17	102.44	235	Compliant
2	Pipe	66.90	77.99	205	Compliant
	Hanger support	95.17	103.84	235	Compliant

equivalent stress is shown in Figures 14, 15. As shown in Figure 14, when m is 0.1 and 0.2, the flow rate of the valve increases rapidly at the beginning of opening, resulting in a large sudden change in fluid momentum. This momentum is transferred to the pipeline, and an average equivalent stress rises rapidly, and a double-peak pattern corresponding to the fluid pressure wave is formed during the valve opening stage. When m is 1 and 2, although the stress rises slowly at the beginning of valve opening, at the end of valve opening, due to the concentrated release of fluid kinetic energy within a short period of time, the stress peak significantly increases. In contrast, when m is 0.2, 0.25, and 0.5, the change in valve opening degree is more coordinated with the flow rate growth rate, allowing the fluid momentum to be distributed more uniformly in time, thereby significantly reducing the amplitude of the pressure wave and reducing the peak stress of the pipeline. The system exhibits a more stable response characteristic. Correspondingly, the same pattern is also observed in the different valve opening characteristics on the support and hanger.

From the combined results of Figures 14, 15, it can be seen that due to the combined influence of the compressibility of natural gas and the non-linearity of the valve, appropriately increasing the initial flow increment at the valve opening can slow down the growth rate of the flow at the end, thereby balancing the change of fluid momentum over time and making the pressure and stress responses more stable. Among them, the system performs the best when $m = 0.25$. The strength verification results for the main part of the system are shown in Table 8. The results indicate that all the main load-bearing components meet the safety requirements.

4 Conclusion

This paper takes the natural gas supply system of a 300 MW F-class heavy-duty gas turbine as the research object, analyzing the pneumatic hammer effect during the valve opening and closing

process of the system and the transient response characteristics of the structure. Based on the combined simulation of computational fluid dynamics and transient structural dynamics, a complete fluid–structure coupling dynamic model of the natural gas pipeline was established. The propagation laws of internal pressure and the transient structural response under different valve opening times and opening characteristics were systematically investigated under rated operating conditions, which represent the most critical transient scenario for gas turbine operation. The main conclusions are as follows:

1. The pneumatic hammer phenomenon in the natural gas pipeline system exhibits the characteristic of ‘no initial peak and long-term decay’. The compressibility of the gas causes the pressure wave to gradually accumulate during the valve opening process rather than erupting instantaneously. The peak occurs mostly when the valve is approaching full opening, accompanied by sparse waves and interference resulting in multi-period decay oscillations. Compared with the liquid system, the waveform of the gas pneumatic hammer is smoother and decays more slowly.
2. The valve opening time and the opening characteristics jointly determine the intensity of the pneumatic hammer effect and the level of structural response. When the opening time is short ($\Delta t = 0.2$ s), the sudden increase in flow leads to a significant transient peak overpressure (the overpressure is approximately 5.7%); when $\Delta t \geq 0.6$ s, the peak drops to below 3.945 MPa. Extending the opening time can smooth the change in fluid momentum and significantly reduce the pressure and stress peaks. At the same time, the opening characteristic factor m plays a decisive role in the response pattern: combined with the flow characteristic of the valve ‘first slow then fast’, the ‘first fast then slow’ type opening ($m < 1$) forms a double-peak low-pressure response, while the ‘first slow then fast’ type ($m > 1$) generates a single-peak high-pressure at the end. Appropriately increasing the initial opening rate growth

and slowing down the final growth ($m \approx 0.25$) can balance the momentum distribution over time, making the system pressure and stress fluctuations the most stable.

3. The structural dynamic response of the pipeline exhibits phase differences and amplification effects. The overall safety is good, but some parts need to be strengthened. The pipeline stress and pressure wave respond synchronously, while the hanger support has a lag of approximately 0.2 s and interferes with the pipeline load, showing a higher oscillation frequency and greater amplitude of dynamic amplification characteristics. The coupling analysis indicates that the maximum stress is concentrated at the single-hole pad plate of support 13 and the edge of the hanger. Except for these localized stress concentration regions, the stresses in the main load-bearing components of the pipeline and supports remain below the allowable limits, indicating overall structural safety under the investigated operating conditions. Strengthening measures at elbows and hanger connection regions are recommended to further enhance the shock resistance margin.

In conclusion, for the gas turbine start-stop and load regulation process where the valve flow characteristic is ‘first slow then rapid’, the engineering suggestion is as follows: The “fast start and slow opening” valve strategy ($m \approx 0.25$) should be given priority, and the opening time ($\Delta t \geq 0.6$ s) should be reasonably extended to smooth the change in fluid momentum, weaken the peak pressure wave, and reduce the structural dynamic response, thereby enhancing the safety and reliability of heavy-duty gas turbines operation.

Data availability statement

The original contributions presented in the study are included in the article/supplementary material, further inquiries can be directed to the corresponding author.

Author contributions

LX: Writing – original draft, Methodology, Conceptualization. PC: Validation, Writing – original draft, Formal Analysis. GL: Writing – original draft, Visualization, Validation, Investigation. NW: Data curation, Investigation, Formal Analysis, Writing – original draft. JS: Validation, Data curation, Writing – original draft. GX: Writing – review and editing, Project administration,

References

- Davies, W., Wolf, M., Barry, M., O’Hern, S., and Morse, T. (2021). The effect of valve closure time on water hammer. *ASME International Mechanical Engineering Congress Exposition*, V010T10A026. doi:10.1115/IMECE2021-71153
- Di, N. C., Urbanowicz, K., Michele, S., Celli, D., Pasquali, D., and Di Risio, M. (2025). On water hammer waves. *Wave Motion* 134, 103507. doi:10.1016/j.wavemoti.2025.103507
- Ding, H., and Ji, J. C. (2023). Vibration control of fluid-conveying pipes: a state-of-the-art review. *Appl. Math. Mech.* 44 (9), 1423–1456. doi:10.1007/s10483-023-3023-9
- Ding, S. Y., Zhang, Q. D., and Lu, X. C. (2024). Impact of valve closing time on water hammer effect considering the comprehensive factors of pipeline length and flow velocity. *Chem. Manag.* (29), 161–164. (in Chinese). doi:10.19900/j.cnki.ISSN1008-4800.2024.29.040
- Fan, K. L., Yang, C., Xie, Z. L., and Ma, X. (2021). Load-regulation characteristics of gas turbine combined cycle power system controlled with compressor inlet air heating. *Appl. Therm. Eng.* 196, 117285. doi:10.1016/j.applthermaleng.2021.117285
- Fan, Y. T., Kozul, M., Li, W. P., and Sandberg, R. D. (2024). Eddy-viscosity-improved resolvent analysis of compressible turbulent boundary layers. *J. Fluid Mech.* 983, A46. doi:10.1017/jfm.2024.174
- Henclik, S. (2018). Analytical solution and numerical study on water hammer in a pipeline closed with an elastically attached valve. *J. Sound Vib.* 417, 245–259. doi:10.1016/j.jsv.2017.12.011
- Impram, S., Nese, S. V., and Oral, B. (2020). Challenges of renewable energy penetration on power system flexibility: a survey. *Energy Strategy Rev.* 31, 100539. doi:10.1016/j.esr.2020.100539

Methodology. YM: Supervision, Writing – review and editing, Conceptualization, Software.

Funding

The author(s) declared that financial support was not received for this work and/or its publication.

Acknowledgements

Thanks for the supporting from the scientific research project of Shandong Electric Power Engineering Consulting Institute Corp., Ltd.

Conflict of interest

Authors LX, PC, GL, NW, and JS were employed by Shandong Electric Power Engineering Consulting Institute Corp., Ltd.

The remaining author(s) declared that this work was conducted in the absence of any commercial or financial relationships that could be construed as a potential conflict of interest.

Generative AI statement

The author(s) declared that generative AI was not used in the creation of this manuscript.

Any alternative text (alt text) provided alongside figures in this article has been generated by Frontiers with the support of artificial intelligence and reasonable efforts have been made to ensure accuracy, including review by the authors wherever possible. If you identify any issues, please contact us.

Publisher’s note

All claims expressed in this article are solely those of the authors and do not necessarily represent those of their affiliated organizations, or those of the publisher, the editors and the reviewers. Any product that may be evaluated in this article, or claim that may be made by its manufacturer, is not guaranteed or endorsed by the publisher.

- Islam, M. M., Yu, T., Giannoccaro, G., Mi, Y., la Scala, M., Rajabi Nasab, M., et al. (2024). Improving reliability and stability of the power systems: a comprehensive review on the role of energy storage systems to enhance flexibility. *IEEE Access* 12, 152738–152765. doi:10.1109/access.2024.3476959
- Kaliatka, A., Vaišnoras, M., and Valinčius, M. (2014). Modelling of valve induced water hammer phenomena in a district heating system. *Comput. and Fluids* 94, 30–36. doi:10.1016/j.compfluid.2014.01.035
- Liu, B., Zhao, J. G., and Qian, J. H. (2017). Numerical analysis of cavitation erosion and particle erosion in butterfly valve. *Eng. Fail. Anal.* 80: 312–324. doi:10.1016/j.engfailanal.2017.06.045
- Lema, M., López, P. F., Buchlin, J. M., Rambaud, P., and Steelant, J. (2016). Analysis of fluid hammer occurrence with phase change and column separation due to fast valve opening by means of flow visualization. *Exp. Therm. Fluid Sci.* 79, 143–153. doi:10.1016/j.expthermfluidsci.2016.07.008
- Li, L., Tan, D. P., Yin, Z. C., Wang, T., Fan, X., and Wang, R. (2021). Investigation on the multiphase vortex and its fluid-solid vibration characters for sustainability production. *Renew. Energy* 175, 887–909. doi:10.1016/j.renene.2021.05.027
- Li, Y. Y., Lian, T. Y., Liu, Z. D., Zhang, Y., Shi, X., and Li, W. (2025). Ammonia combustion for gas turbine decarbonation: opportunities, strategies, and challenges. *Proc. Combust. Inst.* 41, 105876. doi:10.1016/j.proci.2025.105876
- Liu, B. (2015). *Dynamic excitation simulation and dynamic performance optimization of marine gearbox*. Chongqing: Chongqing University. (in Chinese).
- Luo, X. M., Yang, R. Q., Wu, Q. H., and Zhang, D. (2025). Hydraulic transient analysis in low gas-liquid ratio pipelines under valve closure conditions: pressure surge characteristics and predictive modeling. *J. Pipeline Sci. Eng.*, 100376. doi:10.1016/j.jpse.2025.100376
- Menter, F. R. (1994). Two-equation eddy-viscosity turbulence models for engineering applications. *AIAA Journal* 32 (8), 1598–1605. doi:10.2514/3.12149
- Mo, X. Y., Zheng, Y., Kan, K., Zhang, H. S., and Pan, H. (2021). Influence of different valve closing rules and outlet form on pipeline water hammer. *J. Drainage Irrigation Machinery Engineering (JDIME)* 39 (04), 392–396. (in Chinese). doi:10.3969/j.issn.1674-8530.19.0203
- Plouraboué, F. (2024). Review on water-hammer waves mechanical and theoretical foundations. *Eur. J. Mech. - B/Fluids* 108, 237–271. doi:10.1016/j.euromechflu.2024.08.001
- Ren, X. W., Li, P., and Chen, H. Y. (2020). Numerical simulation of water hammer in liquid methane feedline based on two compressible fluid models. *Cryogenics* 109, 103122. doi:10.1016/j.cryogenics.2020.103122
- Riasi, A., and Tazraei, P. (2017). Numerical analysis of the hydraulic transient response in the presence of surge tanks and relief valves. *Renew. Energy* 107, 138–146. doi:10.1016/j.renene.2017.01.046
- Ricci, M., Pacciani, R., Macelloni, P., Cecchi, S., Bettini, C., and Marconcini, M. (2021). An automated strategy for gas turbines off-design predictions with a CFD-based throughflow method. *Appl. Therm. Eng.* 192: 116783. doi:10.1016/j.applthermaleng.2021.116783
- Verástegui, F., Lorca, Á., Olivares, D., and Negrete-Pincetic, M. (2021). Optimization-based analysis of decarbonization pathways and flexibility requirements in highly renewable power systems. *Energy* 234, 121242. doi:10.1016/j.energy.2021.121242
- Versteeg, H., and Malalasekera, W. (2010). *An introduction to computational fluid dynamics*. India: Pearson.
- Xin, Q. L., Du, J. Y., Liu, M. S., Hu, J. K., Yu, W., Yuan, F. Y., et al. (2024). Experimental study on the effects of two-stage valve closure on the maximum water hammer pressure in micro-hydroelectric system. *J. Water Process Eng.* 65, 105886. doi:10.1016/j.jwpe.2024.105886
- Yao, E., Kember, G., and Hansen, D. (2015). Analysis of water hammer attenuation in applications with varying valve closure times. *J. Eng. Mech.* 141, (1) 04014107. doi:10.1061/(asce)em.1943-7889.0000825
- Yao, N. N., Pan, W. G., Zhang, J. K., and Wei, L. (2024). The advancement on carbon-free ammonia fuels for gas turbine: a review. *Energy Convers. Manag.* 315: 118745. doi:10.1016/j.enconman.2024.118745
- Yin, Z. C., Ni, Y. S., Li, L., Wang, T., Wu, J., Li, Z., et al. (2024). Numerical modeling and experimental investigation of a two-phase sink vortex and its fluid-solid vibration characteristics. *J. Zhejiang University-SCIENCE A* 25 (1), 47–62. doi:10.1631/jzus.a2200014
- Zha, C. Y., Pan, C. R., Sun, Z. L., and Liu, Q. (2024). Reliability sensitivity analysis for water hammer-induced stress failure of fluid-conveying pipe. *Appl. Math. Model.* 130, 51–65. doi:10.1016/j.apm.2024.02.028
- Zhang, Y., Xi, Z. D., and Sun, L. (2022). Numerical investigation of water hammer effect in pipeline of NPP considering two-phase compressible flow. *Prog. Nucl. Energy* 150, 104287. doi:10.1016/j.pnucene.2022.104287
- Zhao, Z. X., Duan, Z. D., Sun, H. R., and Xue, H. X. (2025). Numerical modelling of water hammer induced by two phase flow with large temperature difference. *CIESC J.* 76 (S1), 170–180. (in Chinese). doi:10.11949/0438-1157.20241187